DUAL WING, SWEPT FORWARD SWEPT REARWARD WING, AND SINGLE WING
DESIGN OPTIMIZATION FOR HIGH PERFORMANCE BUSINESS AIRPLANES

Mark D. Rhodes[*] and Bruce P. Selberg[+]
University of Missouri-Rolla
Rolla, Missouri

ABSTRACT

An investigation was performed to compare closely coupled dual wing and swept forward swept rearward wing aircraft to corresponding single wing "baseline" designs to judge the advantages offered by aircraft designed with multiple wing systems. The optimum multiple wing geometry used on the multiple wing designs was determined in an analytic study which investigated the two- and three-dimensional aerodynamic behavior of a wide range of multiple wing configurations in order to find the wing geometry that created the minimum cruise drag. This analysis used a multi-element inviscid vortex panel program coupled to a momentum integral boundary layer analysis program to account for the aerodynamic coupling between the wings and to provide the two-dimensional aerodynamic data, which was then used as input for a three-dimensional vortex lattice program, which calculated the three-dimensional aerodynamic data. The low drag of the multiple wing configurations is due to a combination of two dimensional drag reductions, three dimensional drag reductions, tailoring the three dimensional drag for the swept forward swept rearward design, and the structural advantages of the two wings that because of the structural connections permitted higher aspect ratios.

NOMENCLATURE

S	= stagger (in chord lengths)
S_r	= stagger (in chord lengths) at the wing root
S_t	= stagger (in chord lengths) at the wing tip
G	= gap (in chord lengths)
G_r	= gap (in chord lengths) at wing root
G_t	= gap (in chord lengths) at wing tip
D	= decalage angle
D_r	= decalage angle at root
D_t	= decalage angle at tip
α	= wing angle of attack
c	= wing chord
b	= wing span
S_{ref}	= wing reference area
AR	= aspect ratio, b^2/S_{ref}
λ	= taper ratio, C_{tip}/C_{root}
R_c	= Reynolds number based on wing chord

R	= Reynolds number per meter or foot
C_p	= pressure coefficient, $(p - p_\infty)/q_\infty$
x/c	= nondimensional chordwise location
C_l	= sectional lift coefficient
C_L	= total lift coefficient
$C_{L_{cr}}$	= cruise lift coefficient
C_d	= sectional drag coefficient
C_D	= total drag coefficient
C_{D_i}	= induced drag coefficient
$C_{D_{cr}}$	= cruise drag coefficient
C_l/C_d	= sectional lift-to-drag ratio
L/D	= total lift-to-drag ratio
$(L/D)_{cr}$	= cruise lift-to-drag ratio
C_{l_α}	= sectional lift curve slope
V_{cr}	= cruise speed
P_{cr}	= cruise power
D_{cr}	= cruise drag
W_{cr}	= cruise weight
ΔD_i	= percent reduction in induced drag

INTRODUCTION

With the advent of the all-metal aircraft wing, the biplane and triplane wing designs used on most of the early aircraft were replaced by a single wing surface which was structurally stronger and aerodynamically "cleaner" than the multi-surface wings it replaced. Progressively lighter and more powerful aircraft engines and higher flight speeds obviated the need for the additional wing area provided by the multi-surface wings. However, more recent studies have shown that both closely coupled dual wing systems and swept forward swept rearward systems possess aerodynamic advantages over the single wing configuration that could lead to multiple wing aircraft designs that are more fuel efficient than single wing designs by virtue of the lower drag of the multiple wings.

The three main factors affecting the performance of a closely coupled dual wing system with the same airfoils and equal chords are stagger, S, the longitudinal separation of the wings; gap, G, the vertical distance between the wings; and decalage, D, the relative angle between the two wings. Both stagger and gap are measured from mid-chord to mid-chord and nondimensionalized with respect to chord length, c. Gap is always positive,

stagger is positive when the upper wing is ahead of the lower wing, and decalage is positive when the upper wing is at a higher angle of incidence than the lower wing. Figure 1 shows the geometric relationships of these parameters.

The first research into the aerodynamics of biplane systems was conducted by Norton [1] in 1918. Norton conducted wind tunnel tests with cambered three-dimensional airfoils, using a dual wing configuration of a constant gap of 1.0, a constant zero degree decalage angle, and a stagger that varied from -1.0 to +1.0 in 0.25 increments. His results indicated that the +1.0 stagger configuration produced the highest performance of any stagger in the range investigated, and that a positive stagger restrained the movement of the center of pressure.
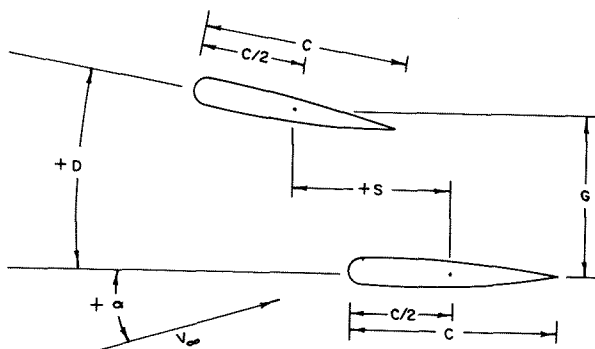
NOTE: S and G are nondimensionalized with respect to C

FIGURE 1. Dual Wing Geometric Relationships

Knight and Noyes [2,3,4] performed the same tests in 1929, except that gap and decalage were also varied. Their research revealed that non-zero decalage tended to decrease the maximum lift coefficient. They also found that in decreasing the proximity of the wings, by increasing stagger or gap or both, the effects of aerodynamic coupling diminished, which caused the loads on each wing to become more similar.

In 1936, Nenadovitch [5] conducted two-dimensional tests with dual wing configurations and with the equivalent single wing. His tests showed that a stagger of 1.0, a gap of 0.33, and a decalage of -6 degrees achieved the greatest increase in performance over the equivalent single wing. All three of these optimum configuration parameters were at the extreme end of the range of values investigated.

Analytical procedures developed in 1934 by Prandtl and Tietjens [6] determined that some dual wing configurations would have lower induced drag than an equivalent single wing.

Olson and Selberg [7], in 1974, compared dual wings and single wings of the same lift capacity in experiments with three-dimensional models. Their findings showed that dual wing configurations could achieve substantially higher lift-to-drag ratios than a single wing due to the much lower drag coefficient of the dual wing.

Also in 1974, Smith [8] discussed analytical results of investigations of multi-component airfoils, including dual wing systems, in an effort to obtain higher maximum lift coefficients. However, he did not investigate multi-element systems which would improve the lift-to-drag ratio by finding a minimum drag configuration under cruise conditions. Thus, his findings contributed little to the problem of maximizing cruise performance with dual wing systems.

In 1980, Rokhsaz and Selberg [9], also using analytical methods, determined that dual wing systems could reduce two-dimensional drag by 13% or more over an equivalent single wing. In addition, they extensively investigated the mechanisms which caused this phenomenon.

The current study is intended first to find the dual wing and the swept forward swept rearward configurations which attain the greatest performance improvements over a single wing, using two state-of-the-art airfoil sections, the MS(1)-0313 [10] and the laminar NL(S)-0715F [11], which has recently been given the official NASA designation of NLF-0215F. The second phase of this study involves the design and performance comparison of several single wing "baseline" aircraft and of corresponding dual wing aircraft and swept forward swept rearward aircraft to determine the advantages and disadvantages of these multi-wing aircraft designs.

The 13% thick turbulent flow MS(1)-0313 airfoil is an improved version of the LS(1)-0413 (GA(W)-2) airfoil. The NL(S)-0715F airfoil is a 15% thick natural laminar flow airfoil designed for a cruise lift coefficient of 0.2 at a Reynolds number of 9×10^6. The NL(S)-0715F airfoil has a 20% chord simple flap at the trailing edge, which is deflected upward 10 degrees during cruise. Figure 2 shows the shapes of these airfoils.

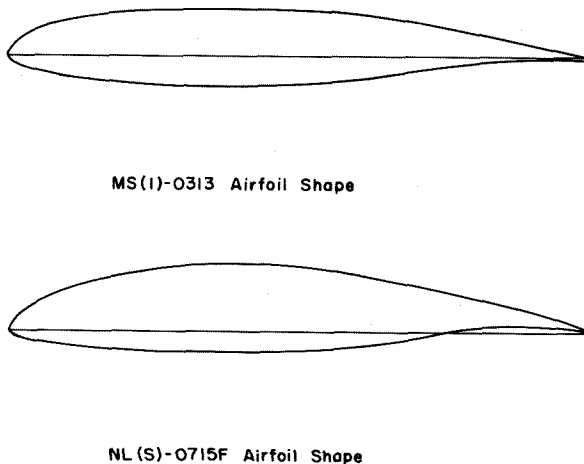MS(1)-0313 Airfoil Shape

NL(S)-0715F Airfoil Shape

FIGURE 2. MS(1)-0313 and NL(S)-0715F Airfoil Shapes

DUAL AIRFOIL TRADEOFF STUDIES

A detailed parametric study was conducted to analytically determine the combination of stagger, gap, and decalage which resulted in the greatest improvement in the wing lift-to-drag ratio, L/D, in terms of both two-dimensional viscous drag and three-dimensional induced drag results. For small staggers the results of Rokhsaz and Selberg [9] in-

dicated that the most favorable configuration, on the basis of only two-dimensional performance, was a stagger of 1.0, a gap of 0.26, and a decalage of -6 degrees for the NACA 63_2-215 airfoil. Using this placement of the airfoil system as the starting point for the two airfoils considered in this study (the MS(1)-0313 and the NL(S)-0715F), the parametric investigation was performed by holding the initial values of two of these parameters constant while changing the value of the third variable.

The parametric study utilized an inviscid vortex panel multi-element program joined to a momentum integral boundary layer analysis program to compute theoretical two-dimensional viscid and inviscid data. The laminar flow portion of the momentum integral program predicts the behavior of the boundary layer with Thwaites' method [12] and uses Michel's transition criterion[13] to determine the point of laminar-turbulent transition. The turbulent flow solution is then obtained by Head's momentum integral method[14] and the viscous drag is calculated with the Squire-Young formula [15]. Viscous drag predictions from the combined vortex panel viscous boundary layer program were compared to experimental results[10,11] known at the same Reynolds numbers to determine the degree of correlation between experimental and analytical results. Figure 3 compares the theoretical to the experimental data for the MS(1)-0313 airfoil at a Reynolds number, R_c, of 4×10^6 and for the NL(S)-0715F at a Reynolds number of 6×10^6. This good agreement was achieved by using a Young's factor of 2.4 for the MS(1)-0313 and 2.2 for the NL(S)-0715F in the Squire-Young equation. Similarly good results for both airfoils were obtained at other Reynolds numbers. The boundary layer program was also tested with Granville's transition criterion[16], but the correlation diverged at the lower lift coefficients. The results of these programs were used as input to a three-dimensional vortex lattice program, which calculated the induced drag of the various configurations. The UMR vortex lattice program predicts higher values of induced drag than NARUVLE[17], which consistently underestimates induced drag[18]. A typical case for an untwisted straight wing of aspect ratio 12 is presented in Figure 4, as predicted by NARUVLE and the UMR vortex lattice program.
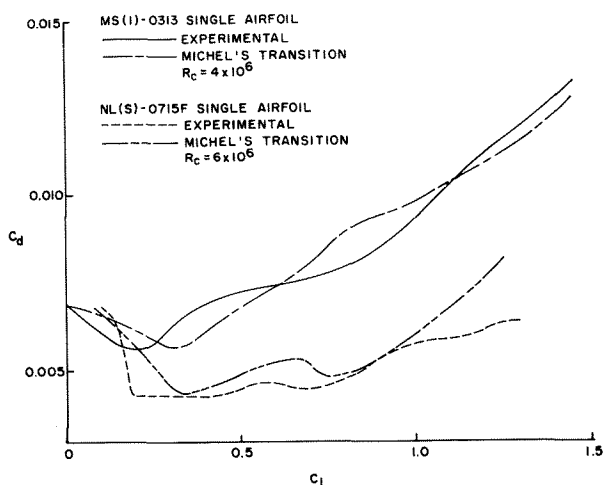
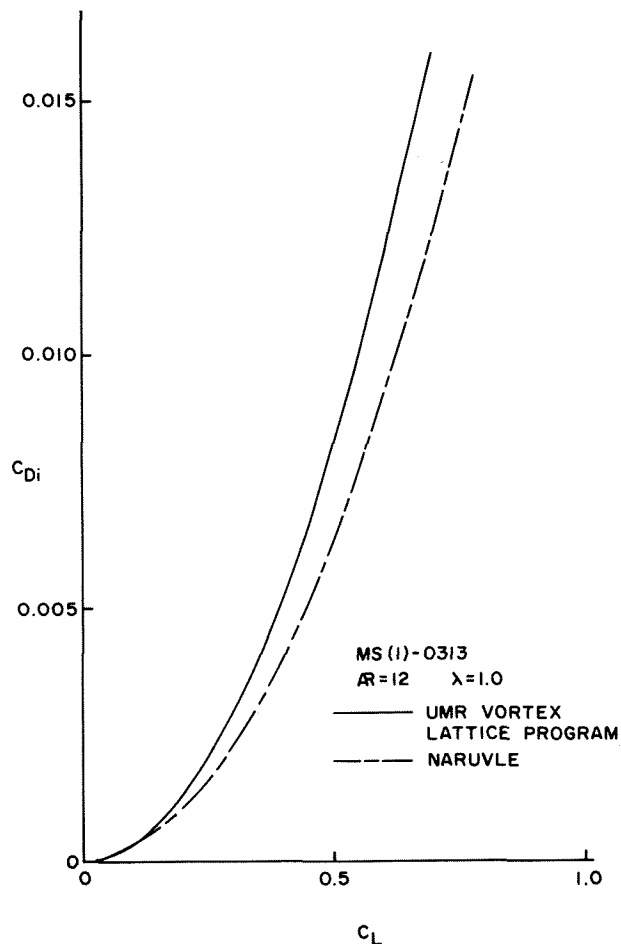FIGURE 3. Comparison of Theoretical With Experimental Results

FIGURE 4. Vortex Lattice Program Comparison

Initial investigation of the performance of various dual wing configurations covered a wide range of staggers to confirm the observations of previous dual wing research[5,7,9]. Figures 5 and 6 present the findings of this investigation and a comparison with the single wing data for the MS(1)-0313 airfoil. In Figure 5, the negative stagger runs (curves E through H) invariably exhibited flow separation at relatively low lift coefficients, while the positive stagger, negative decalage cases (curves B through D) delayed the separation point to lift coefficients of 1.5 or greater. The positive stagger, positive decalage run (curve A) separated at a lift coefficient of less than 0.8, and produced an excessive amount of drag, as Figure 6 shows. Likewise, the negative stagger configurations created large amounts of drag in relation to the positive stagger, negative decalage cases. All of these findings supported the conclusions reached by Norton[1], Nenadovitch [5], and Olson and Selberg[7], who determined that both the negative stagger and the positive decalage configurations performed poorly compared with the positive stagger, negative decalage condition. The NL(S)-0715F airfoil displayed similar behavior.

With the negative stagger and the positive decalage cases rejected for their poor performance, the stagger, gap, and decalage angle changes were varied to find the optimum configuration. In previous research, this optimum for small staggers has been found to occur at a point where the two wing
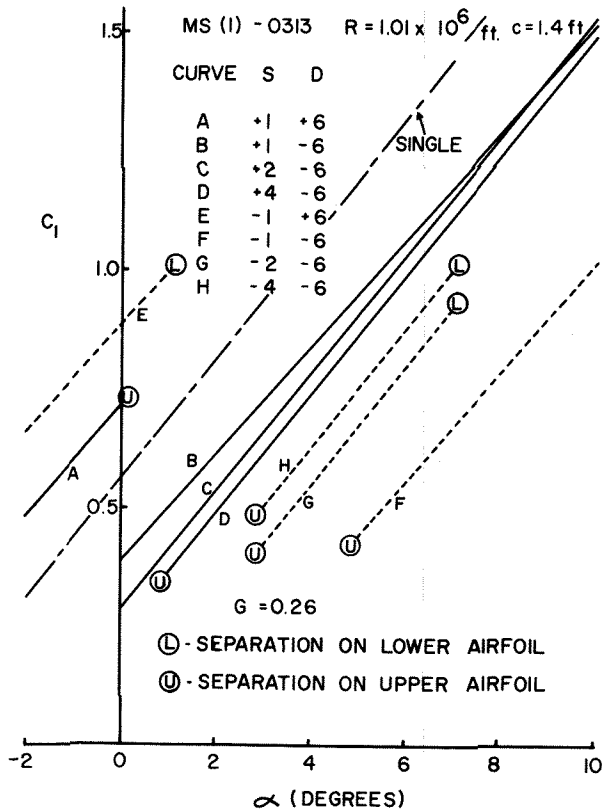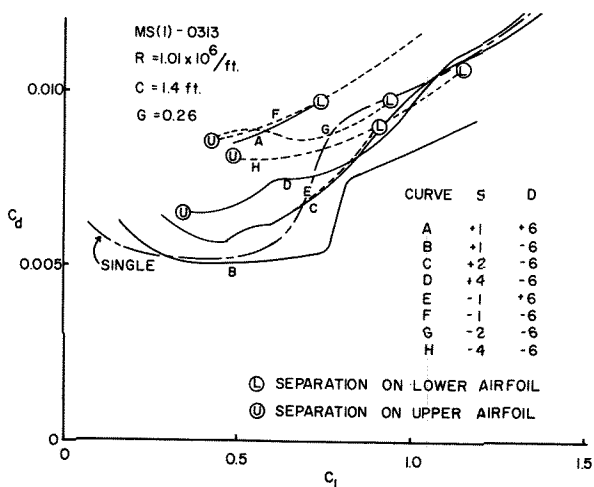
FIGURE 5. Dual Wing Two-Dimensional Lift Curves

FIGURE 6. Dual Wing Two-Dimensional Drag Polars

FIGURE 7. Effects of Stagger on Two-Dimensional Aerodynamic Coupling for the MS(1)-0313 Airfoil

surfaces are highly coupled aerodynamically. Figure 7 shows the degree of aerodynamic coupling between two MS(1)-0313 airfoils, as denoted by the ratio of the lift curve slope, C_{l_α}, of the two surfaces. The peak coupling occurred at a stagger of 1.0 for the 0.26 gap and -6 degree decalage case, which agrees well with the research done by Nenadovitch[5] and Rokhsaz and Selberg[9]. This coupling decreases very rapidly with minor coupling existing for staggers greater than or equal to 5.0. Thus, for the swept forward swept rearward configuration two dimensional effects will only be significant near the outboard section of each wing section where the staggers are less than 5.0.
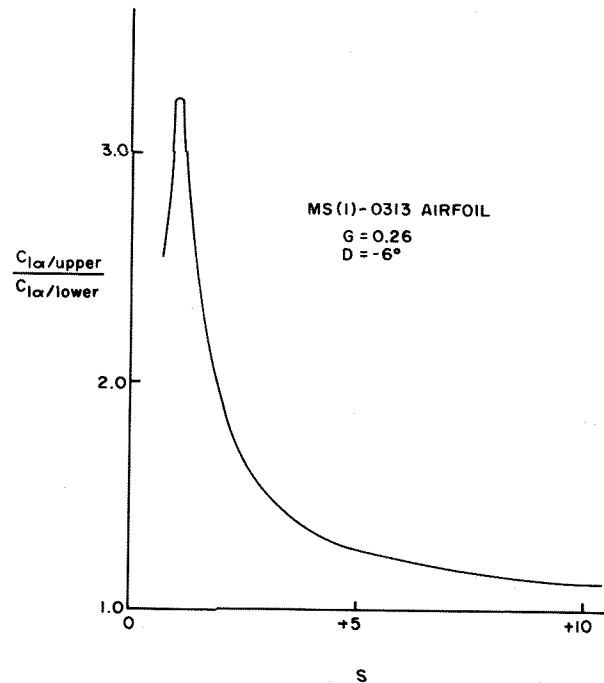
Figure 8 shows the pressure distribution for

two airfoil sections that are closely coupled; a stagger of 1.0, a gap of 0.26, and a decalage of -6 degrees. For the case with 1.0 stagger, 0.26 gap, and -6 degree decalage, the lower wing at a geometric angle of attack, α, of 1 degree obtained a lift coefficient, C_l, of 0.439, comparable to that of a single wing at a -1 degree angle of attack. The upper wing produced a lift coefficient of 0.559 at a geometric angle of attack of -5 degrees, which is approximately equal to the lift on a single wing at a zero degree angle of attack. Thus, the upper and lower wings receive a +5 degree and a -2 degree induced angle of attack, respectively, indicating that the flow about each wing is greatly affected by the presence of the other wing. Figure 8 also illustrates the reduced leading edge pressure peak and the reduced adverse pressure gradient experienced by the dual wings, both of which inhibit boundary layer separation.

Results of the parametric study for the MS(1)-0313 airfoil are shown in Figures 9 through 14. Figure 9 depicts the two-dimensional results of the constant gap, constant decalage, variable stagger runs and, for comparison, the single wing performance. A significant increase over the single wing C_l/C_d curve was obtained with staggers of 1.0 and 1.1. Performance fell off as stagger was increased or decreased from this optimum stagger range. For a stagger of 4.0 the dual results are inferior to those of the single airfoil. Looking back at Figure 7, it can be seen that the optimum configuration occurred at the point of maximum aerodynamic coupling. For all cases, gap was held at 0.26 and decalage was a constant -6 degrees.

The two-dimensional variable gap analysis is summarized in Figure 10. With stagger and decalage held at 1.0 and -6 degrees, respectively, the highest performance was obtained at gaps of 0.10 and 0.26. Lift-to-drag ratios dropped considerable as
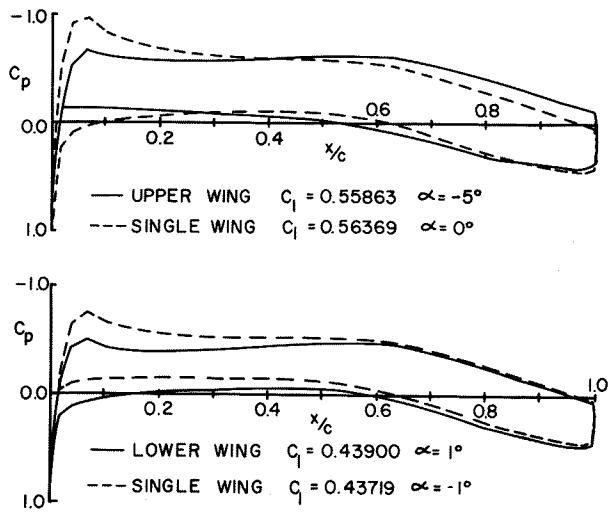
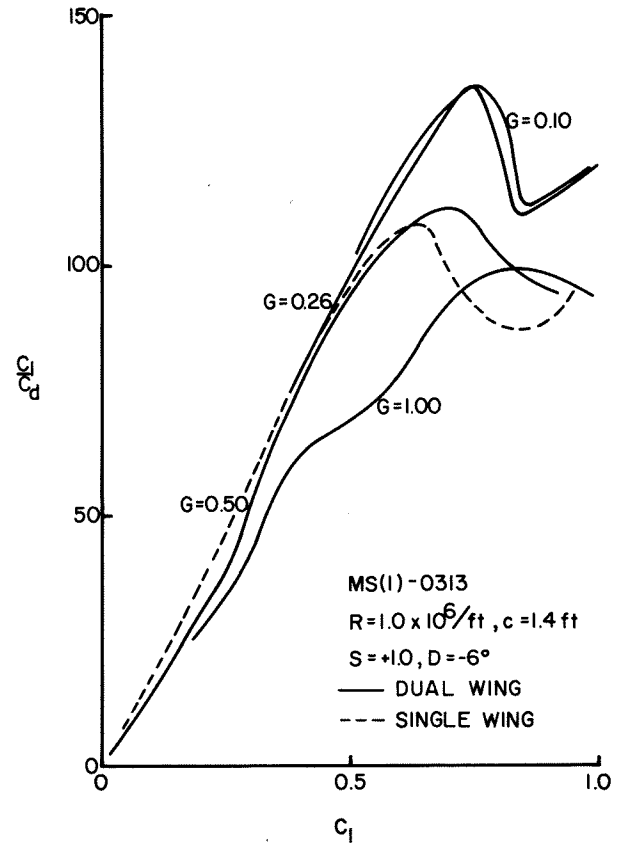FIGURE 8. Single and Dual Wing
Pressure Distributions

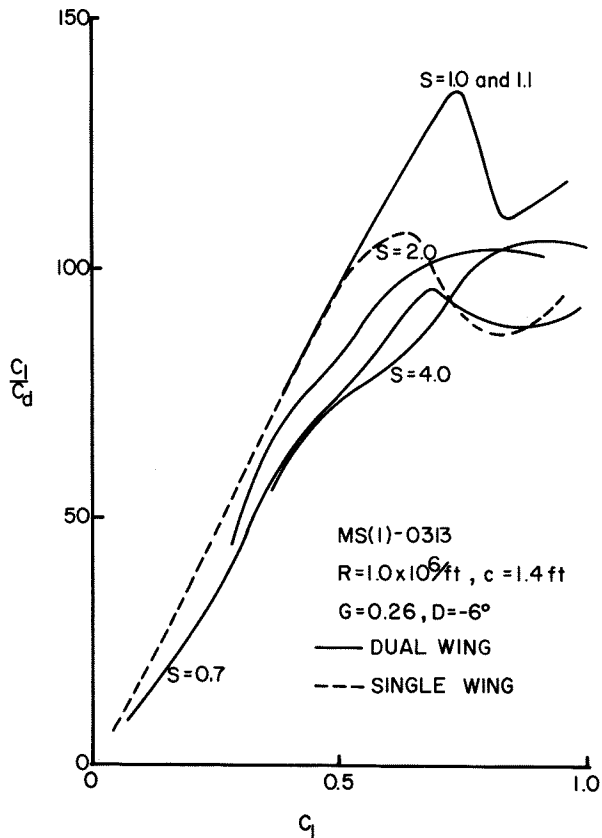FIGURE 9. MS(1)-0313 Two Dimensional
Stagger Study Results

FIGURE 10. MS(1)-0313 Two-Dimensional
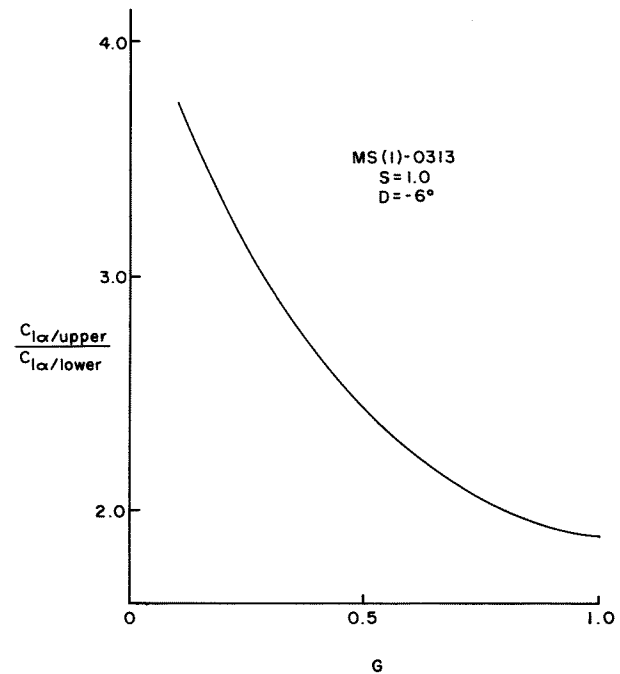Gap Study Results

FIGURE 11. Effects of Gap on Two-Dimensional
Aerodynamic Coupling for the
MS(1)-0313 Airfoil

gap increased beyond 0.26. Figure 11 shows that
the aerodynamic coupling effects became much more
pronounced as the gap decreased, a situation
analogous to that experienced with stagger. The
optimum gap cases thus corresponded to positions of
high aerodynamic coupling.

500

Figure 12 presents the data for the variable decalage two-dimensional runs. Overall, the best small stagger performance was obtained with a -6 degree decalage. A -8 degree decalage produced a higher maximum lift-to-drag ratio than did the -6 degree decalage case, but the latter held the performance edge at lift coefficients of 0.5 and below. All the decalage cases shown exhibited transition behavior that was superior to that of a single wing, as Figure 13 illustrates for a decalage of -6 degrees. The transition points for both the dual wing and the single wing configurations were at about 60% and 10% chord for low and high lift coefficients, respectively. However, the shift from transition at 60% chord to transition at 10% chord occurred at lift coefficients of 0.6 to 0.8 for the single wing, as opposed to 0.9 to 1.1 for the dual wing configuration. The essence of this behavior is that the dual wing benefits from a considerably longer period of laminar flow between lift coefficients of 0.6 and 1.1 and a corresponding decrease in viscous drag. The swept forward wing configuration will benefit from these effects only near the tips of the wings.
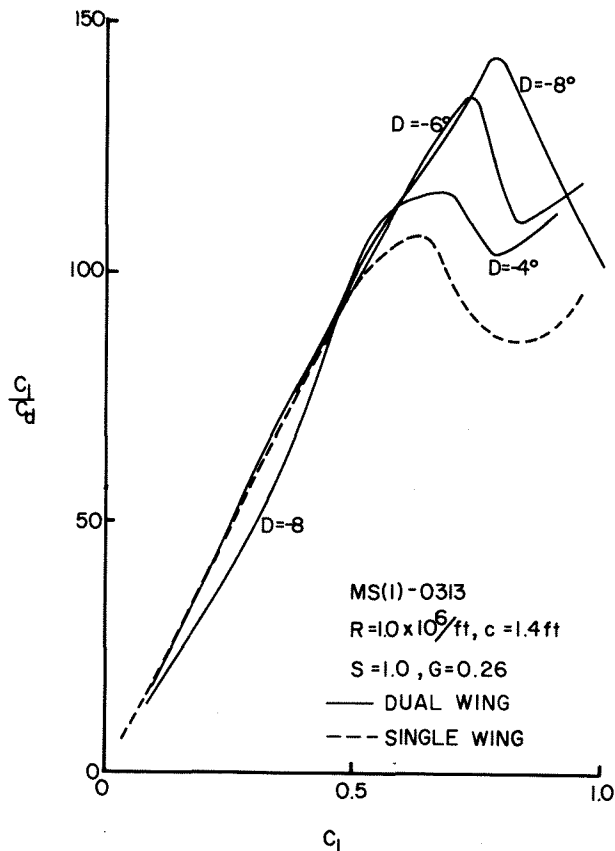

FIGURE 12. MS(1)-0313 Two-Dimensional Decalage Study Results

FIGURE 13. MS(1)-0313 Transition Points

Induced drag comparisons between the various configurations were also conducted, using the three-dimensional vortex lattice program. The results of this study indicated that the difference in induced drag between various dual wing configurations was much less than the corresponding difference in two-dimensional drag, as much as 70-90% less, over the range of stagger, gap, and decalage investigated. The study covered wings of as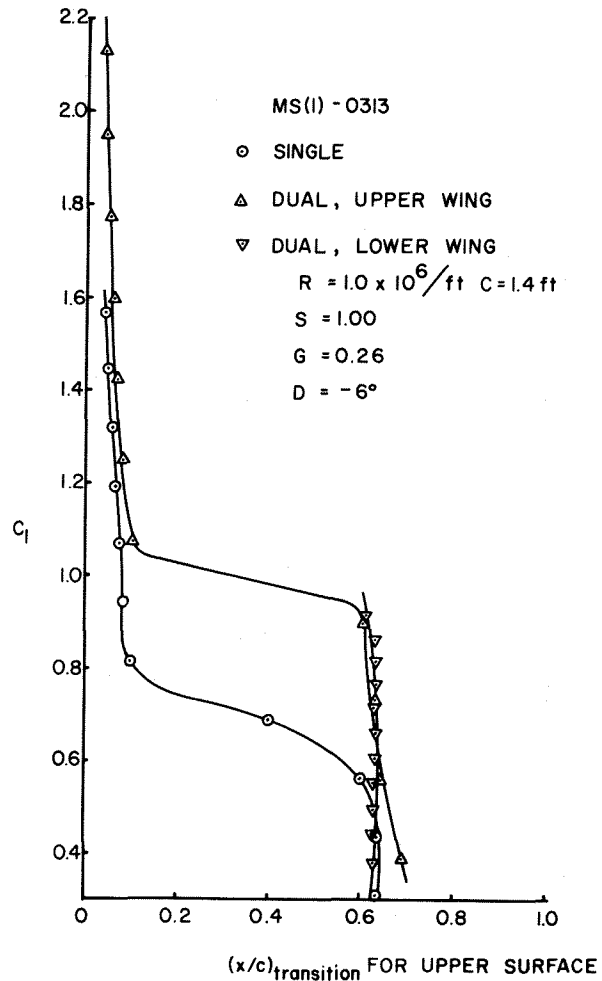pect ratios 12 and 16. Figure 14 shows a sample of the cases investigated, and illustrates the slight induced drag advantage of the dual wing over a single wing of equivalent aspect ratio, i.e. a single airfoil with the same span, b, and area, S_{ref}, as the dual wing, and whose chord is equal to the sum of the two dual wing chords. The figure also indicates the significantly lower induced drag of the aspect ratio 16 wing compared to the wing of aspect ratio 12.

On the basis of these two-dimensional viscous drag and three-dimensional induced drag results, the optimum dual wing configuration was determined to be a stagger of 1.0, a gap of 0.26, and a decalage of -6 degrees. The 0.10 gap case, which showed marginally better results than the 0.26 gap case, was not chosen since it was felt that flow blockage effects between the upper and lower airfoils might be significant at such a low gap, and the vortex panel program used for the two-dimensional viscid and inviscid data is unable to predict the consequences of such blockage.

Induced drag calculations for the swept forward swept rearward wing configuration are shown in Figure 15 as a function of the stagger at the wing root section. These results illustrate the benefits of lower staggers at the wing root. Figure 16 illustrates the effect of wing twist on induced drag with the tip geometry being that of
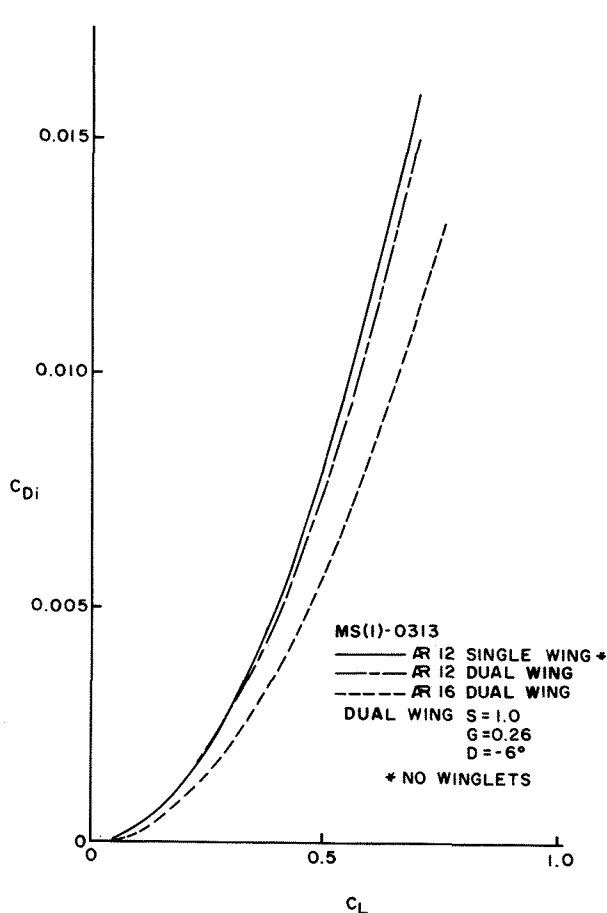
FIGURE 14. Typical Induced Drag Curves for the MS(1)-0313 Airfoil

FIGURE 15. Induced Drag for the Swept Forward Swept Rearward Configuration at Various Staggers

the optimum dual wing case. A geometric washout of 6 degrees between root and tip provided the lowest induced drag. The effects of taper are shown in Figure 17 with a constant chord wing having the lowest induced drag. This appears to be caused by the effects of the favorable two dimensional coupling that occurs near the wing tips and hence more pronounced with larger chords in that location.

The two dimensional parametric study was also conducted with the NL(S)-0715F airfoil section. The same trends were found to occur except at much higher lift coefficients. Figure 18 illustrates the delay in transition provided by the -6 degree decalage case over the single wing. This transition delay was significant and extended over a wide range of lift coefficients, which supports the findings obtained with the MS(1)-0313 airfoil. In contrast to the MS(1)-0313, however, the NL(S)-0715F dual wing transition delay did not become appreciable until lift coefficients greater than 1.0 were obtained. This is because so much of the NL(S)-0715F surface is laminar up to lift coefficients of 1.0 and the coupling cannot produce a significantly greater laminar run. Above lift coefficients of 1.0 the dual airfoil improvements were again realized, although not to as great an extent. From the two-dimensional results for the NL(S)-0715F airfoil section the optimum configuration for the wing was a stagger of 1.0, a gap of 0.26, and a decalage angle of -6 degrees.
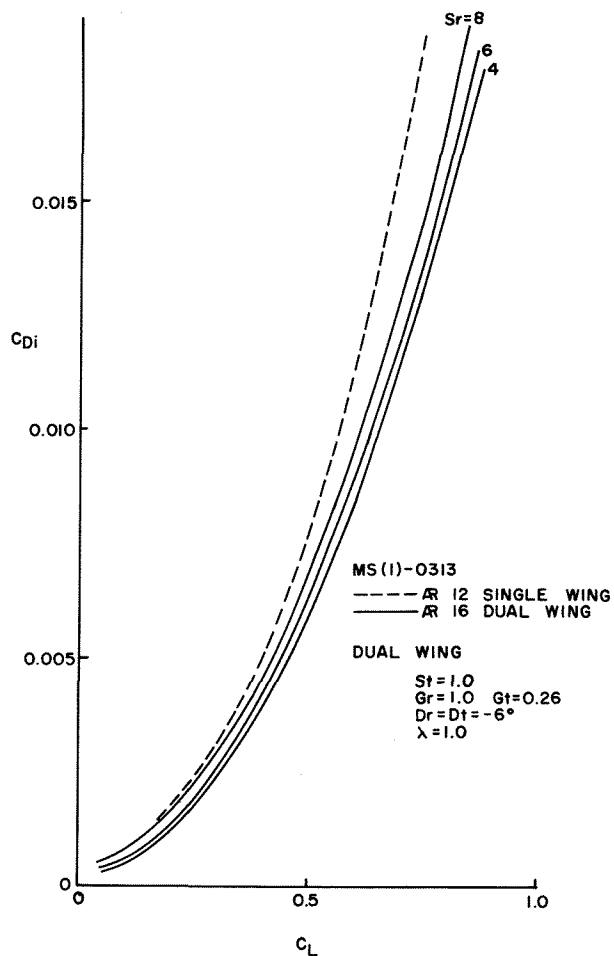
The induced drag trends followed those of the MS(1)-0313 airfoil section. The performance figures produced by this parametric study were used to design six aircraft: a six-place and a twelve-place "baseline" aircraft, and a six-place and a twelve-place dual wing aircraft, and a six-place and a twelve-place swept forward swept rearward aircraft. The two baseline aircraft were of conventional single wing, aft tail configuration and were used as reference points. The dual wing aircraft and the swept forward swept rearward aircraft which used the same fuselage, tail, and power plant as the corresponding baseline aircraft, were compared to these reference points to ascertain the merits of these multi-wing aircraft designs. Each of the six designs was evaluated with both the MS(1)-0313 and the NL(S)-0715F airfoil sections.

DESIGN OF THE BASELINE AIRCRAFT

The six aircraft in this study were designed for a 563 km/hr (350 mi/hr) cruise speed at altitudes of 9144-12192 m (30-40,000 ft) and a range of 2414 km (1500 mi) or more. The baseline aircraft were limited to aspect ratios of six to twelve and wing loadings of 1197-2873 N/m^2 (25-60 lb/ft^2). For each wing configuration, two separate aircraft designs were required, both a six-place and a twelve-place airplane. The six-place aircraft was
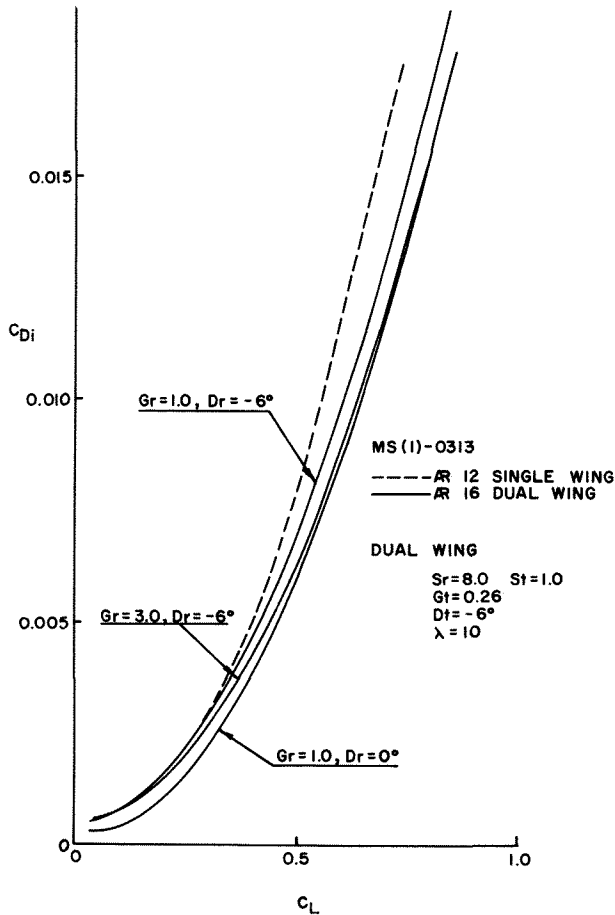
FIGURE 16. Effect of Twist on Induced Drag for the Swept Forward Swept Rearward Configuration

FIGURE 17. Swept Forward Swept Rearward Taper Ratio Results

designed for a 5338 N (1200 lb) payload and was intended as a personal or small business airplane, while the twelve-place aircraft, with twice the payload of the six-place, was meant to compete in the business aircraft market. All the aircraft in this study were designed with lifting surfaces made of composite materials.

The design procedure began by sizing of the fuselage. The height and width of the six- and twelve-place fuselages were sized to present minimum frontal area, and thus create minimum drag, while providing ample interior volume for pilot, passengers, and luggage. The width of the twelve-place fuselage was also influenced by the requirement for a 30.5 cm (12 in) aisle between the seats. The seat pitch, or the distance between adjacent rows of seats, was set at 91.4 cm (36 in) for both versions. The passenger and luggage compartment for each version was then enclosed in a pressure vessel designed to provide a cabin pressure latitude of 2438 m (8000 ft) at an actual altitude of 12192 m (40,000 ft). The rest of each fuselage was sized to provide space for the landing gear, power-plant, avionics, and environmental control unit. No space was required for the fuel, since the fuel tanks were placed in the wings.

The six-place fuselage was built around a 132 cm (52 in) high, 112 cm (44 in) wide, 4.42 m (14.5
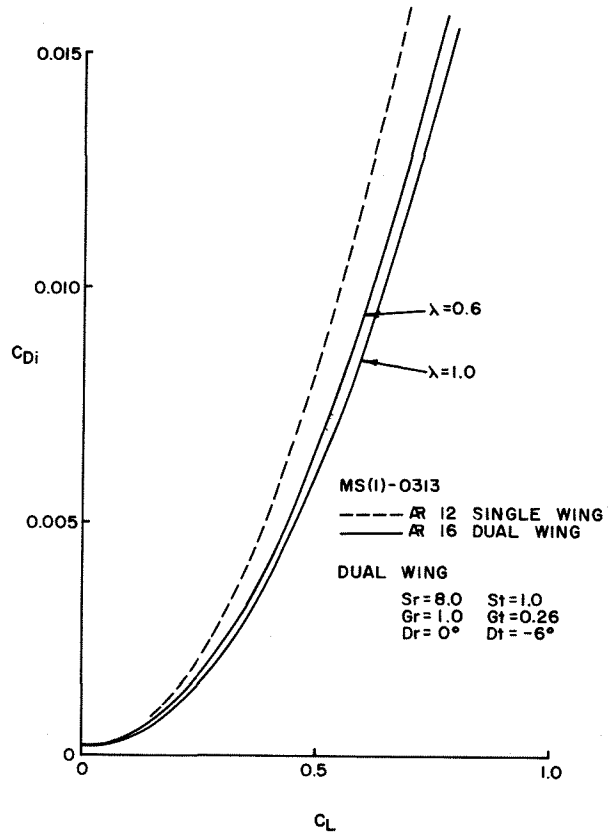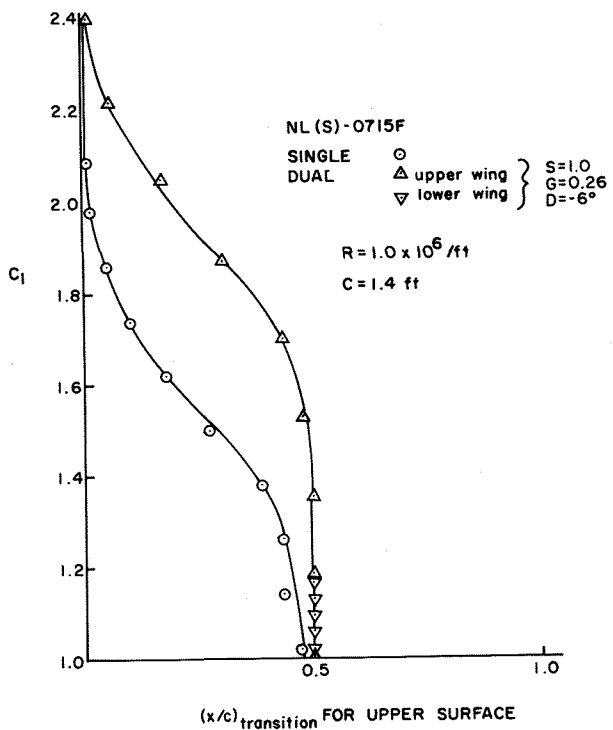

FIGURE 18. NL(S)-0715F Transition Points

ft) long pressure cabin containing the six seats (in three rows of two seats each) and a luggage

503

area aft of the last row of seats. The fuselage was designed for a conventional tricycle landing gear arrangement, with the nose gear housed below and forward of the pressure cabin and with the main gear located below and aft of the luggage compartment. The main gear retract aft into the fuselage. The single turboprop engine was buried in the aftmost section of the fuselage tail cone. Air inlets for the engine were situated on either side of the fuselage and the propeller shaft was extended through the aft fuselage. The avionics and the environmental control unit were also housed in the fuselage aft of the pressure cabin.

The twelve-seat fuselage consisted of six rows of two seats and a baggage compartment aft of the last seat row. A 30.5 cm (12 in) center aisle was also provided. The passenger and cargo area was enclosed by a 163 cm (64 in) high, 163 cm (64 in) wide, and 7.37 m (24.2 ft) long pressure vessel. The tricycle gear were placed in the same relative positions as were the landing gear for the six-place fuselage. The two turbofan engines were mounted on horizontal pylons attached to the aft fuselage. The avionics and environmental control unit were placed in the aft fuselage.

The six-place aircraft used a scaled version of the Pratt and Whitney PT6-A45A turboprop engine[20] with a 2.29 m (90 in) diameter four-bladed propeller. Specific fuel consumption was assumed to be a constant 0.344 kg/hW-hr (0.55 lb/hp-hr). The twelve-place aircraft used twin turbofan engines scaled from engines from a General Aviation Turbine Engine (GATE) study[21]. A 0.061 kg/N-hr (0.6 lb/lb-hr) thrust specific fuel consumption was assumed. The turboprop engine weight was scaled by the ratio of required power to production power, while the turbofan engine weight was scaled by the ratio of required thrust to reference engine thrust.

Each baseline design required two versions, one with the MS(1)-0313 airfoil and one with the natural laminar airfoil, the NL(S)-0715F. The two- and three-dimensional performance of each airfoil type was predicted with the same programs used in the multi-wing stagger, gap, and decalage studies.

All baseline aircraft were designed to utilize winglets to reduce the induced drag. The magnitude of this induced drag reduction was determined in a computer tradeoff study which found the optimum wing taper ratio, λ, the ratio of tip chord to root chord.

A computer winglet study was conducted on a wing of aspect ratio 12 with taper ratios of 0.2 to 1.0, using the NARUVLE vortex lattice program to compute the induced drag of the various configurations. Using a NASA winglet study[21] as a guide, the dihedral and incidence of the winglets was varied to find the configuration that provided the greatest reduction in induced drag. The optimum configuration agreed with Reference 21 in terms of dihedral and incidence, although the magnitude of the predicted drag reduction was less. Because of the high degree of correlation between the current study and the NASA study, it was decided to use the standard NASA winglet design of Reference 21. To be conservative, the drag reduction value obtained from NARUVLE was used, rather than that of Reference 21. The re-

sults, which are corrected to include the additional parasite drag of the winglets, are shown in Figure 19, and indicated that taper ratios of 0.6 and 0.8 produced the greatest reduction in induced drag, ΔD_i. Since it was expected that the cruise lift coefficient would be 0.4 or higher, the 0.8 taper ratio was selected over the 0.6 taper ratio. The results of the winglet study were then used to modify the induced drag values from the UMR vortex lattice program to account for the effects of adding winglets.

Aircraft weight estimates were obtained with the aid of equations from Nicolai[22] and Torenbeek[23,24] and from a UMR design project[25], a four-place high speed general aviation aircraft, that utilized NASTRAN prediction methods.

Using equations from Nicolai with the UMR four-place design as a reference aircraft, the fuselage and empennage weights were determined for the six- and twelve-place aircraft under consideration. Nicolai's equations were used as scaling factors on the reference weights by taking into account the different fuselage dimensions, take-off weights, and other pertinent factors. Wing weights were estimated from a modification of Torenbeek's formula to account for the composite wings, and, for the dual wing aircraft, the dual wing configuration[26], which structurally connects the two wings at root, tip, and first bending moment (i.e., mid-span). These modified wing weight formulas were checked against the results of Reference 27 and showed good agreement. An ultimate load factor of 5.7, calculated from a 3.8g load with a factor of safety of 1.5, was used. Estimates for engine weight were obtained by scaling up the reference aircraft engine weight, using as a scaling the ratio of required thrust to the references aircraft required thrust. Weights of landing gear, avionics, electrical and fuel systems, and other equipment on board were estimated with Nicolai's equations. The weight of the required fuel was extrapolated from the reference aircraft, based on the different aircraft weights and ranges.
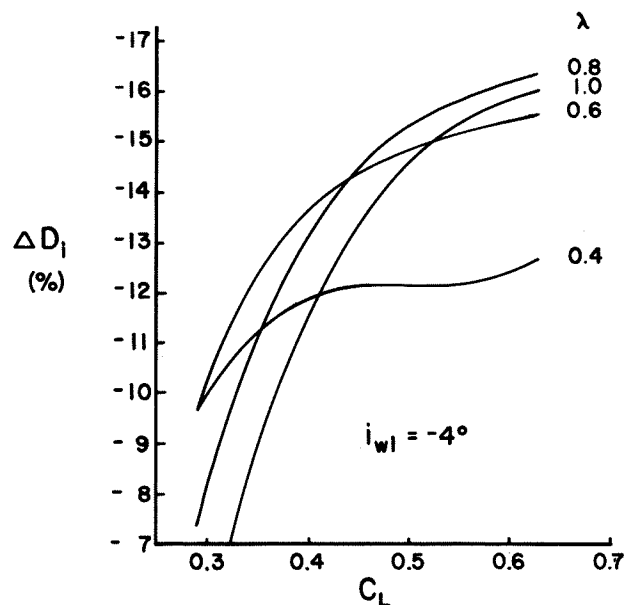

FIGURE 19. Induced Drag Reduction Due to Winglets

Estimates of total aircraft drag coefficient were obtained by the component buildup method. The drag coefficients of each component, weighted by the ratio of the component area to the aircraft reference area, were totalled and multiplied by 1.1 to account for interference effects, as suggested in Reference 28.

The drag of the lifting surfaces, the wing and horizontal tail, was predicted with the momentum integral boundary layer and the vortex lattice programs described above. For each cruise lift coefficient being investigated, the viscous drag at the proper Reynolds number and the induced drag at the desired aspect ratio, taper ratio, and sweep angle were added to get a total wing drag coefficient. A factor of 0.0005, or five to ten percent of the zero-lift drag coefficient for the airfoils under consideration, was added to this wing drag coefficient to account for interference.

Graphs and equations for turbulent flow about streamlined bodies from Roskam[28], Hoerner[29], and Crawford[30] were used to estimate the drag contributions of essentially non-lifting components such as the fuselage, nacelles, and vertical tail. These drag coefficients, separately weighted by the ratio of component reference area to the aircraft reference area, were then added to get the total drag coefficient due to non-lifting components. To account for interference drag, this drag coefficient was increased by ten percent.

The wing area was then optimized. A computer code would scan through a range of wing areas to find the area which created the least cruise drag. For each wing area in the desired range, the program computed the total aircraft cruise weight, W_{cr}, assuming constant engine weight which determined the cruise lift coefficient. The program then searched through the two- and three-dimensional drag polars to find the viscous and induced drag coefficients of the wing at the desired lift coefficient for the specified conditions, namely cruise Reynolds number and aspect ratio. The drag of the non-lifting components was computed and adjusted for interference effects and added to the wing drag, also adjusted for interference. Minimization of this final drag value was the criterion by which the program selected the optimum wing area. At this point, it should be noted that all aircraft designed for this study were optimized for cruise performance only. No attempt was made to take into account takeoff, climb, or landing performance, since this study is concerned solely with the performance in cruise.

Figure 20 shows a sample of the results of the optimization program for the six-place aircraft with wings of MS(1)-0313 section and aspect ratios of 8 and 12. Over a wing area range of 7 to 28 m^2 (75 to 301 ft^2), the minimum cruise drag was obtained at an area of 13.84 m^2 (149.0 ft^2) for the aspect ratio 8 wing and 12.65 m^2 (136.2 ft^2) for the aspect ratio 12 case. The figure also indicates the significant drag reduction achieved by increasing the aspect ratio from 8 to 12. Figure 21 is the locus of the minimum drag points for the six-place aircraft with the MS(1)-0313 airfoil at the altitudes and aspect ratios given. The figure graphically illustrates the lower drag produced
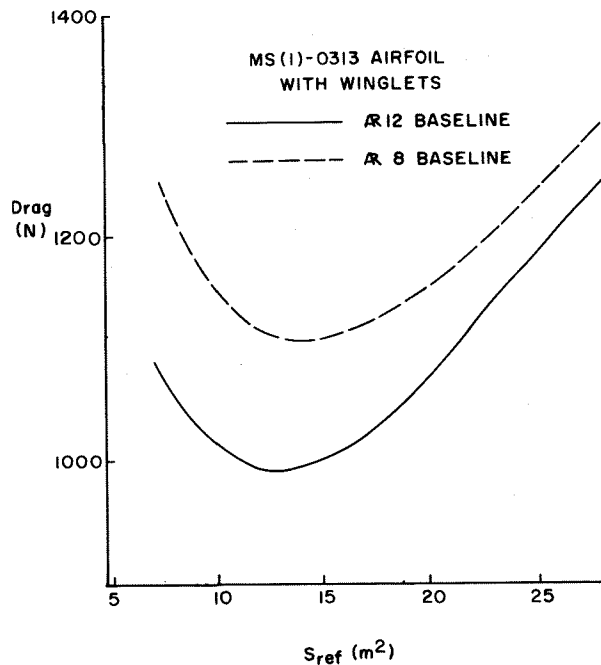

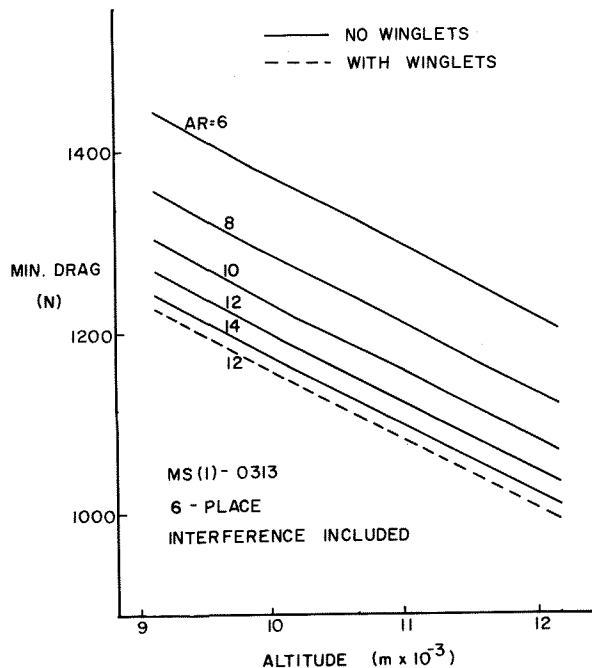FIGURE 20. Six-Place Baseline Aircraft, Sample Optimization Curve

FIGURE 21. Six-Place Baseline Aircraft, Variation of Minimum Drag With Altitude

when the aspect ratio is increased, altitude is increased, or winglets are added. Similar results were found for the twelve-place aircraft and for the NL(S)-0715F airfoil section.

On the basis of the results of the optimization program, a cruise altitude of 12192 m (40,000 ft) was selected as being the best cruise altitude. An aspect ratio of 12 was chosen for its low minimum drag values. The aspect ratio 14 cases were

505

run for comparison purposes only, since the base-
line aircraft were arbitrarily limited to aspect
ratios of 12 or less.

After the optimum wing areas were determined,
a final sizing of the horizontal and vertical
tails was required to provide longitudinal, later-
al, and directional stability. With the center of
gravity placed at its most unfavorable position,
the horizontal and vertical tail areas were varied
until each aircraft was statically stable. The
degree of static stability attained was comparable
to that found in typical light and business air-
craft. The static stability analysis was per-
formed using the techniques of Roskam[31,32].

Once the horizontal tail size was known, the
trimmed performance of each aircraft was estimated.
The required tail lift coefficient for zero pitch-
ing moment in cruise was computed, and this tail
lift coefficient was used to find the tail drag
coefficient at the trimmed condition, using the
momentum integral boundary layer and vortex lat-
tice programs described above. This additional
trim drag was calculated, and the untrimmed data
obtained from the optimization program was
modified accordingly.

Table 1 gives these final results of the
baseline design process, as well as the perfor-
mance of a typical current-technology six-place
aircraft[19] for comparison purposes. For both
the six- and twelve-place designs and for both
airfoil sections, the table gives the estimated
cruise weight, drag, power, and lift and drag
coefficients at trimmed cruise conditions. Also
shown is the ratio of lift to drag in cruise for
each aircraft. The last two columns provide the
wing area and estimated range.

The lift-to-drag ratios achieved by these
baseline were markedly higher than most contempo-
rary light and business aircraft. Holmes and
Croom[19] indicate that current technology six-
place have maximum lift-to-drag ratios of about
14 at 556 km/hr (300 kt) cruise speeds. The

baseline six-place aircraft in the current study
attained cruise lift-to-drag ratios of more than
18 at 563 km/hr (350 mi/hr), or more than a 25%
improvement. This much improved performance can
be attributed to the superior airfoil sections
used on the baseline aircraft as well as to the
higher aspect ratios found on the aircraft of
this study. The addition of winglets to the base-
line aircraft also contributed to their superior
performance. However, the rather high wing load-
ings of the baseline aircraft may lead to exces-
sive stall speeds without careful attention to
high lift devices to improve low-speed performance.

Figure 22 shows the exterior views of the
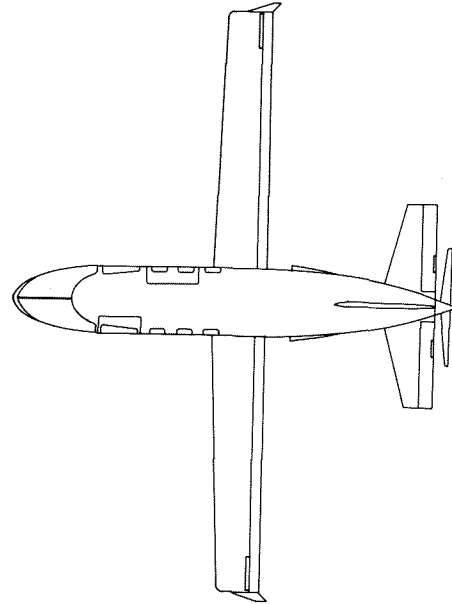finished six-place baseline aircraft.

FIGURE 22. Baseline Exterior Views

TABLE 1. BASELINE DESIGN PERFORMANCE

|	W_{cr} N(lb)	D_{cr} N(lb)	P_{cr} kW(hp)	$C_{L_{cr}}$	$C_{D_{cr}}$	$(L/D)_{cr}$	S_{ref} $m^2(ft^2)$	RANGE km(mi)
MS(1)-0313 Airfoil								
6-Place	19149 (4305)	1054 (237)	165 (221)	0.41	0.0225	18.19	12.65 (136.2)	2555 (1588)
12-Place	38182 (8584)	1939 (436)	303 (407)	0.46	0.0233	19.68	22.49 (242.1)	2719 (1690)
NL(S)-0715F Airfoil								
6-Place	19024 (4277)	956 (215)	150 (201)	0.42	0.0227	18.51	12.27 (132.1)	2716 (1688)
12-Place	38213 (8591)	1744 (392)	273 (366)	0.40	0.0185	21.63	25.88 (278.6)	2970 (1846)
Current Technology Aircraft (6-Place)	22400 (5036)	∿1600 (∿360)	∿250 (∿331)	0.33	∿0.0233	∿14	19.14 (206)	∿2011 (∿1250)
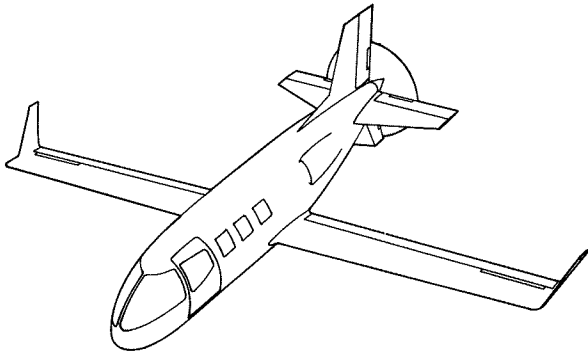
FIGURE 22. Baseline Exterior Views (Continued)

DESIGN OF THE DUAL WING AND SWEPT FORWARD SWEPT REARWARD AIRCRAFT

The six- and twelve-place dual wing and swept forward swept rearward aircraft were designed to meet the same speed, altitude, range, and payload specifications which defined the objectives for the baseline aircraft. However, due to the structural advantages gained by connecting the two wings at points along their span, the dual wing and swept forward swept rearward designs were limited to aspect ratios of 16 or less, rather than 12 as was the case with the baseline aircraft. Aspect ratio was defined as the square of the wing span divided by the total projected area of the two wings.

The multi-wing designs used the same fuselage designs that were used in the baseline aircraft. Minor modifications, such as the addition of a fuselage fuel tank and some rearrangement of internal systems, were the only changes to the baseline fuselages. The fuselage fuel tank was required to supplement the wing fuel tanks, which were too small to hold more than about half the required fuel in the multi-wing aircraft. The multi-wing aircraft also used the same engines as the baseline aircraft.

The multi-wing aircraft, like the baseline aircraft, were designed to use winglets. In the absence of information on the configuration and effectiveness of winglets on multi-wings, it was assumed that the addition of winglets to both multi-wing configurations would reduce the induced drag by approximately half the percentage of drag reduction achieved by winglets on a single wing, which was a conservative estimate of the multi-wing winglet effectiveness. With this assumption, the vortex lattice program was used to find the optimum dual wing taper ratio. A taper ratio of 0.6 was found to create the least induced drag.

Weights of the components of the multi-wing aircraft were identical to those of the baseline aircraft, save for the weight of the wings. The weight of the dual wings was estimated from the modified Torenbeek formula by assuming that each wing carried half the total load on the wings due to the structural connections between the wings. The dual wings were assumed to be connected by structural members at the root, tip, and first bending moment. These members are expected to equalize the loads on the wings, provide greater strength for the wing assembly as a whole, and

minimize the spanwise variations of decalage caused by the twisting of the wings under aerodynamic loading. The swept forward swept rearward wings were connected only at the tip.

The dual wing configuration used the optimum wing placement as determined in the stagger, gap, and decalage study for closely coupled wings. However, since the swept forward swept rearward design lacks a horizontal stabilizer or canard, all longitudinal control forces must be exerted by the wings, which implies the need for a large longitudinal separation between the wings, making larger staggers necessary.

For these reasons the optimum wing configuration, from a combined aerodynamic-stability-control viewpoint, was chosen as the minimum S_{root} which would provide sufficient control power, in the form of $C_{m_{\delta_E}}$. Note that tip configuration was already chosen to be $S = 1$, $G = 0.26$, $D = -6°$, which was the optimum configuration for the closely coupled situation. S_{root} was varied until the swept forward swept rearward design obtained a $C_{m_{\delta_E}}$ that was equal to that of the corresponding baseline designs. This occurred at $S_{root} = 8$. G_r was picked to be 3 to put the wings at the top and bottom of the fuselage respectively.

Drag calculation procedure for the multi-wing configurations was identical to that of the baseline aircraft. The two- and three-dimensional drag polars for both airfoils were obtained from the results of the dual wing and swept forward swept rearward configuration study.

Sample results of the optimization program runs for the multi-wing six-place aircraft, as well as the corresponding baseline results for comparison, are given in Figure 23, and a complete table of results, after being modified for trim, is shown in Table 2.

Figure 24 and 25 illustrate the finished six-place dual wing aircraft and swept forward swept rearward designs, respectively.

DESIGN COMPARISON AND RECOMMENDATIONS

Comparing Table 1 and 2, one immediately notices the lower cruise drag of the multi-wing configurations. The drag and the required power of the dual wing cases was lower than that of the baseline aircraft by 5-9% for the MS(1)-0313 airfoil and by 3-4% for the NL(S)-0715F airfoil, in spite of the fact that, for three of the four cases shown, the weights of the dual wing aircraft were somewhat greater than the weights of the corresponding baseline aircraft. In terms of range, this means that, for the same fuel, the dual wing aircraft achieved 4-10% more range than the baseline aircraft with the MS(1)-0313 airfoil and up to 4% more range with the NL(S)-0715F airfoil. The drag and the required power of the swept forward swept rearward aircraft was also lower than the baseline by 6-11% for the MS(1)-0313 airfoil and by 5-8% for the NL(S)-0715F airfoil even though the wing weights of the swept forward swept rearward configuration were as much as 29% greater than those of the baseline aircraft. The swept forward swept rearward wing aircraft achieved 6-7% increases in range for the MS(1)-0313 airfoil compared to the base-
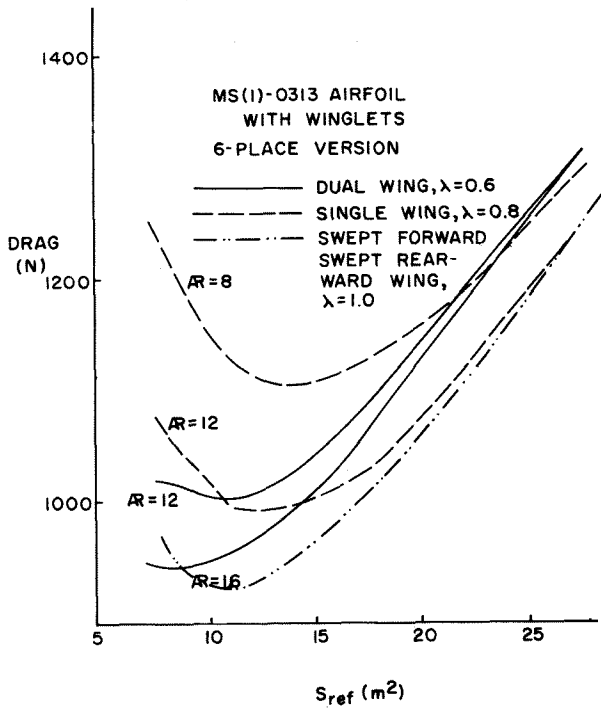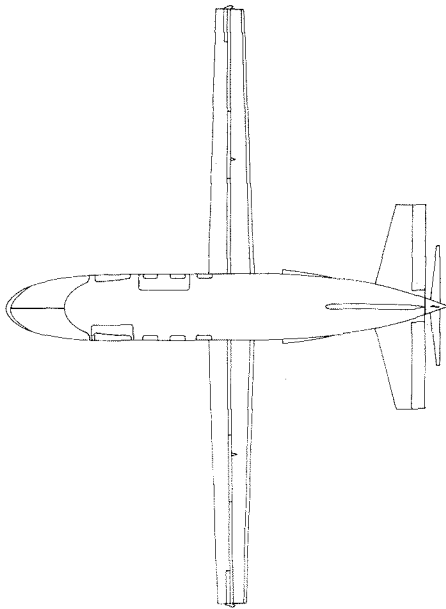
FIGURE 23. Sample Optimization Curves

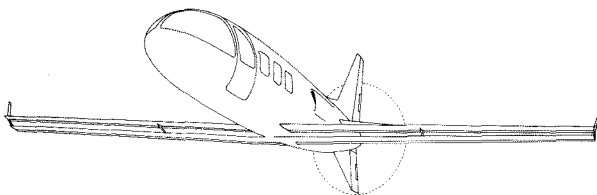FIGURE 24. Dual Wing Design Exterior Views

FIGURE 24. Dual Wing Design Exterior
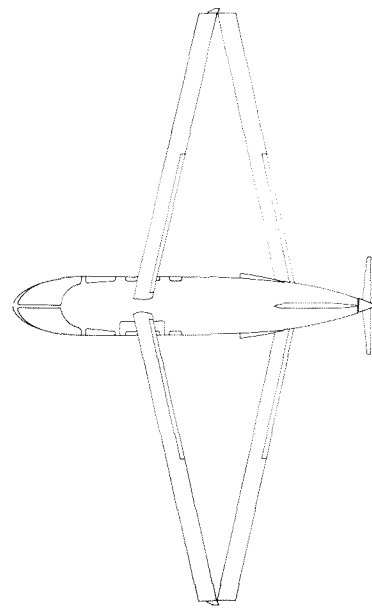Views (Continued)

FIGURE 25. Swept Forward Swept Rearward
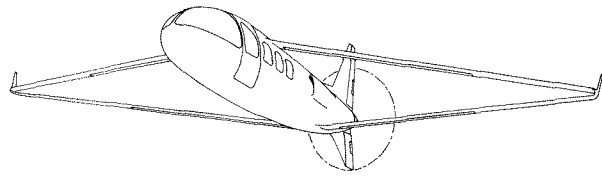Wing Design Exterior Views

FIGURE 25. Swept Forward Swept Rearward Wing
Design Exterior Views (Continued)

line aircraft and 10-14% increases for the NL(S)-
0715F. Furthermore, the lower drag and required
power of the multi-wing aircraft translates to a
lower engine weight for these dual wing designs,
which would make the multi-wing configuration
even more attractive. However, for simplification
purposes, the optimization program assumed a con-
stant powerplant weight. It should also be noted
that the NL(S)-0715F airfoil equipped aircraft ob-
tained a 2-9% drag reduction over the corresponding
aircraft equipped with the MS(1)-0313 airfoil.

Figures 26 and 27 illustrate why the dual
wing aircraft created less drag than the baseline
aircraft. Figure 26 shows a comparison of a single
MS(1)-0313 airfoil and a dual MS(1)-0313 airfoil
at a stagger of 1.0, gap of 0.26, and decalage of
-6 degrees. Even though the drag increased at the
lower left coefficients for the lower Reynolds
number, the dual wing had considerably less drag
at lift coefficients of 0.5 to 0.8. This effect
was found to be negligible for the NL(S)-0715F,
however, due to the fact that the extent of the
laminar flow over the dual wing was not appreciably
greater than that over the single wing at lift
coefficients of less than 1.0.

Figure 27 compares single wings of aspect
ratio 8 and 12 with dual wings of aspect ratio 12
and 16. Both the single and the dual wings utilize
the MS(1)-0313 airfoil. Comparing this figure with

508

TABLE 2. MULTI WING DESIGN PERFORMANCE

	W_{cr} N(lb)	D_{cr} N(lb)	kW(hp)	$C_{L_{cr}}$	$C_{D_{cr}}$	$(L/D)_{cr}$	S_{ref} m²(ft²)	RANGE km(mi)
DUAL WING								
MS(1)-0313 Airfoil								
6-Place	19118 (4298)	1005 (226)	157 (211)	0.65	0.0343	18.99	7.97 (85.8)	2658 (1652)
12-Place	38546 (8666)	1766 (397)	276 (370)	0.57	0.0261	21.85	18.32 (197.2)	2985 (1855)
NL(S)-0715F Airfoil								
6-Place	19215 (4320)	987 (222)	154 (207)	0.51	0.0262	19.47	10.21 (109.9)	2813 (1748)
12-Place	38684 (8697)	1712 (385)	268 (359)	0.47	0.0208	22.58	22.30 (240.0)	2962 (1841)
SWEPT FORWARD / SWEPT REARWARD WING								
MS(1)-0313 Airfoil								
6-Place	19615 (4411)	965 (217)	151 (202)	0.49	0.0241	20.32	10.85 (116.8)	2914 (1811)
12-Place	39440 (8869)	1819 (409)	285 (382)	0.49	0.0226	21.69	21.81 (234.8)	2936 (1826)
NL(S)-0715F Airfoil								
6-Place	19259 (4331)	889 (200)	139 (186)	0.63	0.0292	21.61	8.29 (89.2)	3157 (1962)
12-Place	38750 (8714)	1654 (372)	259 (347)	0.59	0.0252	23.44	17.80 (191.6)	3227 (2006)

MS(1)-0313 AIRFOIL
——— SINGLE WING ($R_c = 3.37 \times 10^6$)
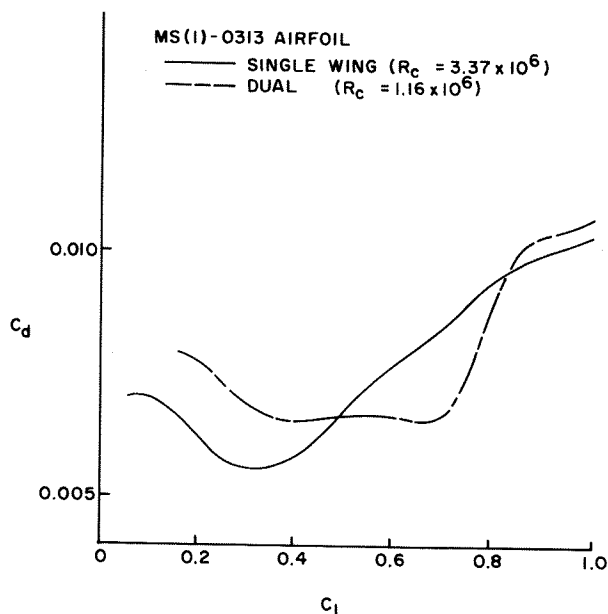– – – DUAL ($R_c = 1.16 \times 10^6$)

FIGURE 26. Single and Dual Wing Two-Dimensional Drag Polars

Figure 14, one notices that the induced drag superiority of the dual wing of aspect ratio 12 over the aspect ratio 12 single wing was negated by the addition of winglets to the configurations. This is due to the assumption that the dual wing winglets would be only half as effective in reducing induced drag as were the winglets on the single wing aircraft. However, while the induced drag was equal in Figure 26 for the aspect ratio 12 cases, the aspect ratio 16 dual wing caused a significant reduction in induced drag over both aspect ratio 12 cases. The NL(S)-0715F airfoil behaved similarly.

The difference in optimum cruise lift coefficient also stands out. The optimum cruise lift coefficients for the baseline aircraft ranged between 0.40 and 0.46, while the dual wing designs optimized at much higher lift coefficients, from 0.47 to 0.65, with correspondingly lower wing areas. These lower wing areas cause higher wing loadings, which bring about higher stall speeds in the dual wing aircraft.

The cause of the higher cruise lift coefficients for the dual aircraft is less obvious. For the six-place MS(1)-0313 aircraft, Figure 28 shows how the cruise lift coefficient increased as the wing aspect ratio increased, due to the steadily decreasing induced drag curve as aspect ratio becomes larger. Looking back at Figures 9,
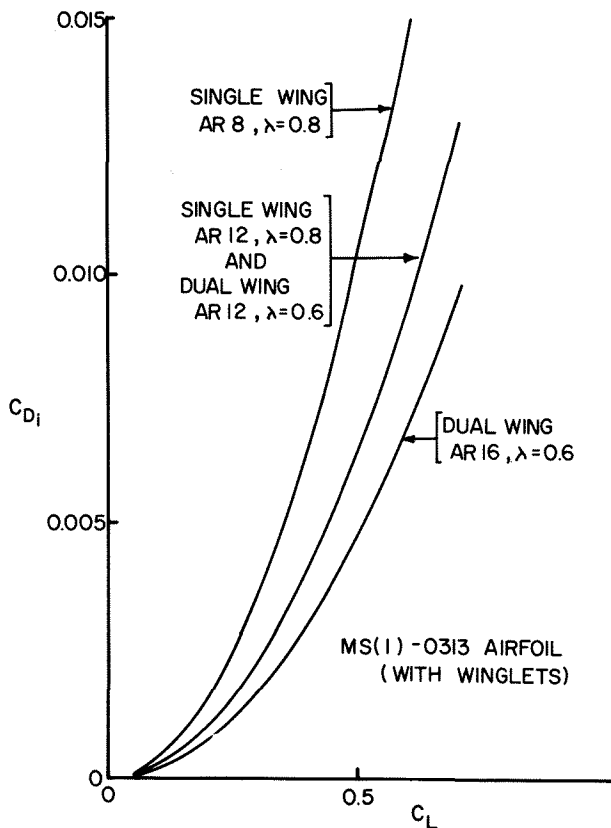
509

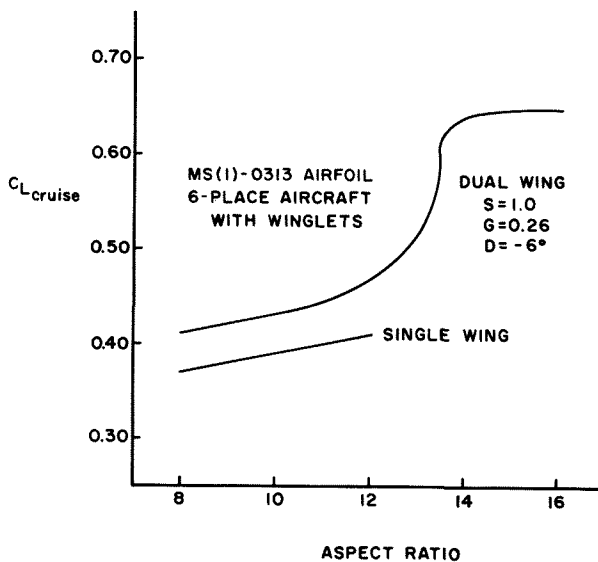FIGURE 27. Single and Dual Wing Induced Drag Polars

FIGURE 28. Variation of Cruise Lift Coefficient with Aspect Ratio

10, and 12, the performance of the dual wing MS(1)-0313 reached its two-dimensional peak at a lift coefficient of about 0.75, which is considerably greater than the cruise lift coefficients for either dual wing MS(1)-0313 aircraft. This, with Figure 28, implies that the two-dimensional performance peak can only be reached by increasing the already large aspect ratio of the dual wing designs. The same can be said of the NL(S)-0715F

aircraft, except that the maximum two-dimensional performance occurs at a lift coefficient of over 1.0.

The swept forward swept rearward design achieved its lower drag over the baseline aircraft due to an optimization of the induced drag with minor trim penalties.

Some potential problems were noted with the multi-wing designs. The first of these, already mentioned previously, is a higher stall speed than the baseline aircraft due to the lower wing areas of the dual wing aircraft. Next, due to the lower projected and sectional wing areas of the multi-wing aircraft, the wing volume available for fuel was insufficient. Thus, while the single wing aircraft could carry all the fuel in the wings, the multi-wing aircraft were required to have a fuselage tank to provide the necessary fuel capacity. Third, the possibility exists that the multi-wing configuration has aeroelastic problems not experienced by the conventional single wing configuration. This possibility was not investigated in this study.

In outperforming the baseline aircraft, the multi-wing designs had to overcome some disadvantages. The greatest disadvantage was the increase in drag coefficient as Reynolds number decreased. Since the wing chords of the multi-wing aircraft were roughly half that of the single wing aircraft, the multi-wing designs were penalized by higher drag coefficients due to the reduced Reynolds number. This disadvantage may be reduced or eliminated by using an airfoil section designed for very low Reynolds number, from about 10^6 to 2×10^6. The two airfoil sections investigated in this study were designed for Reynolds numbers of 6×10^6 to 9×10^6, and suffer from a degradation of performance at lower Reynolds number.

A second disadvantage is the greater structural weight, as calculated by the modified Torenbeek formula, of the multi-wing system. Since this weight estimation formula did not take into account the structural bracing of the inter-wing connections, the favorable structural weight of a dual wing lifting surface was computed to be 3-7% greater than that of a single wing of the same area, aspect ratio, and strength. Comparing a multi-wing of aspect ratio 16 to a single wing of aspect ratio 12, the difference is even greater, on the order of 20% for the dual and 29% for the swept forward swept rearward design, although the larger aspect ratio wing manages a net drag reduction in spite of the weight penalty.

Third, to be conservative, the winglets on the dual wing aircraft were given only half the induced drag reduction achieved by the single wing winglets. This last disadvantage may be removed by extensive research on winglet designs for the dual wing configuration, as has been done for single wing configurations in the past.

For both the single wing and the multi-wing designs, the aircraft weight estimates are conservative. The actual weight of the aircraft was expected to be less than the weight estimated in this study, which would improve the cruise performance of the aircraft.

In spite of these conservative estimates used

510

in the design process, the baseline aircraft designs offer a significant improvement in cruise performance as compared to current technology aircraft. The multi-wing designs, for all their disadvantages, offer still higher cruise performance, and a corresponding decrease in fuel consumption. With further research into the multi-wing aircraft system, such as static and dynamic structural testing, low Reynolds number airfoil design, and dual wing winglet research, the dual wing aircraft should prove to be even more attractive.

REFERENCES

1. Norton, F. H., "Effect of Staggering a Biplane," NACA TN-710, 1918.

2. Knight, and Noyes, R. W., "Wind Tunnel Test on a Series of Biplane Wing Models, Part I. Effects of Changes in Stagger and Gap," NACA TN-310, 1929.

3. Knight, and Noyes, R. W., "Wind Tunnel Tests on a Series of Biplane Wing Models, Part II. Effects of Changes in Decalage, Dihedral, Sweepback, and Overhand," NACA TN-325, 1929.

4. Knight, and Noyes, R. W., "Wind Tunnel Tests on a Series of Biplane Wing Models, Part III. Effects of Changes in Various Combinations of Stagger, Gap, and Decalage," NACA TN-330, 1929.

5. Nenadovitch, M., "Recherches sur les Cellules Biplane Rigides d'Envergure Infine," Publications Scientifiques et Techniques du Minister de L'Air, Institut Aero'-technique de Saint-Cyr, Paris, 1936.

6. Prandtl, L. and Tietjens, O. G., Applied Hydro- and Aeromechanics, Dover Publications, Inc., New York, 1957, pp. 213-216.

7. Olson, E. C. and Selberg, B. P., "Experimental Determination of Improved Aerodynamic Characteristics Utilizing Biplane Wing Configurations," Journal of Aircraft, Vol. 13, April 1976, pp. 256-261.

8. Smith, A. M. O., "High-Lift Aerodynamics," AIAA Paper No. 74-939, 1974.

9. Rokhsaz, K. and Selberg, B. P., "Analytical Investigation of the Aerodynamic Characteristics of Dual Wing Systems," UMR Thesis, Rolla, MO, 1980.

10. McGhee, R. J., "Wind Tunnel Results for a 13-Percent-Thick Medium Speed Airfoil Section," (NASA TM in publication).

11. Somers, D. M., Data on general aviation natural laminar flow airfoil, to be published by NASA.

12. Thwaites, B., "Approximate Calculation of the Laminar Boundary Layer," Aero. Quarterly I, 1949.

13. Michel, R., "Etude de la Transition sur les Profiles d'Aile; Establissement d'un Critere de Determination de Point de Transition et Calcul de la Trainee de Profile Incompressible," ONERA Rept. 1/1578A, 1951.

14. Cebeci, T. and Bradshaw, P., Momentum Transfer in Boundary Layers, Hemisphere Publishing Corp., Washington, 1977, pp. 192-194.

15. Cebeci, T. and Smith, A. M. O., "Calculation of Profile Drag of Airfoils at Low Mach Numbers," Journal of Aircraft, Vol. 5, Nov.-Dec. 1968, pp. 535-542.

16. Granville, P. S., "The Prediction of Transition from Laminar to Turbulent Flow in Boundary Layers on Bodies of Revolution," Tenth Symposium Naval Hydrodynamics, U.S. Government Printing Office, Washington, D.C., 1974, pp. 705-729.

17. Tulinius, J., "Unified Subsonic, Transonic, and Supersonic NAR Vortex Lattice," TFD-72-523, North American Rockwell, Los Angeles, 1972.

18. Paulson, J. W., "Application of Vortex Lattice Theory to Preliminary Aerodynamic Design," National Aeronautics and Space Administration, Langley Research Center, Langley Station, Va., 1976.

19. Holmes, B. J. and Croom, C. C., "Aerodynamic Design Data for a Cruise-Matched High Performance Single Engine Airplane," SAE Paper 810625, 1981.

20. Benstein, E. H. and Smith, R., "Advanced General Aviation Turbine Engine (GATE) Study," NASA CR-159624, 1979.

21. Whitcomb, R. T., "A Design Approach and Selected Wind-Tunnel Results at High Subsonic Speeds for Wing-Tip Mounted Winglets," NASA TN D-8260, 1976.

22. Nicolai, L. M., Fundamentals of Aircraft Design, METS, Inc., San Jose, Calif., 1975, pp. 5.1-5.24, pp. 20.1-20.24.

23. Torenbeek, E., Synthesis of Subsonic Airplane Design, Delft University Press, 1976, pp. 27-76, pp. 263-302, p. 352.

24. Torenbeek, E., "Prediction of Wing Group Weight for Preliminary Design," Aircraft Engineering, July 1971.

25. Hayes, B., Lopez, R., and Rhodes, M., "General Aviation Light Turbo-Powered Aircraft," UMR Senior Design Project, 1980.

26. Cronin, D. L., personal communication, 1981.

27. Anon., Evaluation of Torenbeek's weight estimating formula for a range of aircraft wings, NASA-ARC.

28. Roskam, J., Methods for Estimating Drag Polars of Subsonic Airplanes, published by the author, Lawrence, Kansas, 1971, p. 2.3.

29. Hoerner, S. F., Fluid Dynamic Drag, published by the author, 1965, pp. 6.15-6.19.

30. Crawford, D. R., A Practical Guide to Airplane Performance and Design, 1st ed., Crawford Aviation, Torrance, Calif., 1979, p. 174.

31. Roskam, J., Methods for Estimating Stability and Control Derivatives of Conventional Subsonic Airplanes, published by the author, Lawrence, Kansas, 1971, pp. 21.-12.2.

32. Roskam, J., Airplane Flight Dynamics and Automatic Flight Controls, Part I, Roskam Aviation and Engineering Corp., 1979, pp. 243-377.